The Adhesion Strength of Impact Ice Measured Using a Modified Lap Joint Test

Andrew H. Work Jr.,[1] and Andrew L. Gyekenyesi[2]
Ohio Aerospace Institute, Cleveland, Ohio, 44135, USA

Richard E. Kreeger[3], Jonathan A. Salem[4], Mario M. Vargas[5], and Daniel R. Drabiak[6]
NASA Glenn Research Center, Cleveland, Ohio, 44135, USA

Numerous methodologies have been utilized to measure the adhesion strength of impact ice, and the data reported in the literature varies significantly from test to test. In order to initiate an investigation to determine the cause of this disparity, a new test methodology has been developed and utilized in the Icing Research Tunnel at the NASA Glenn Research Center. Data was obtained while varying the temperature, test section velocity, and cloud droplet mean volumetric diameter. The first data set acquired using this new test method is presented. New trends demonstrate the effect of annealing ice samples, with temperature being a key variable. Observations during the test and analysis of the results suggest the presence of large residual stresses in the samples.

I. Nomenclature

Def12 = *Deflectometer on coupon*
Def6 = *Deflectometer on Serrated Block*
ΔDef = *Difference between two deflectometer readings*
GRC = *Glenn Research Center*
LWC = *Liquid Water Content*
MPa = *Megapascals*
MVD = *Mean Volumetric Diameter*
N = *Newtons*
IRT = *Icing Research Tunnel*
SS = *Stainless Steel*
T_s = *Static Temperature*
T_t = *Total Temperature*
V = *Velocity*
XT Model = *Materials Testing Model*
d = *Days*
h = *Hours*
mm = *Millimeters*
s = *Seconds*
$\Sigma_{\lambda\text{-}\sigma}$ = *Standard deviation of data sans outliers*
Σ_{raw} = *Standard deviation for raw data*
λ_{time} = *Average annealing time*

---

[1] Senior Researcher.
[2] Associate Chief Scientist.
[3] Aerospace Engineer, Icing Branch, AIAA Associate Fellow.
[4] Materials Research Engineer, Ceramic and Polymer Composites Branch.
[5] Research Scientist, Icing Branch, AIAA Associate Fellow.
[6] Research Aerospace Engineer, Icing Branch.

II. Introduction

Studying the adhesion behavior of impact ice is of critical importance when considering aircraft safety, and more specifically, for determining the point at which ice will shed from aircraft surfaces as well as defining the efficacy of de-icing equipment. While adhesion strength of impact ice has been measured in a number of ways since the 1930s, few studies have produced sample sets large enough for statistical analyses. Furthermore, critical information concerning the conditions at which results were obtained, such as the strain rate and surface roughness, are lacking in the majority of the reports currently available in the literature making comparison difficult or impossible.

While individual test methods may exhibit acceptable precision, the combined data in the literature exhibits orders of magnitude of scatter due to the use of vastly different and competing techniques [1]. Furthermore, conflicting trends exist in the literature. The two most prevalent trends are both exhibited in the data of Raraty and Tabor [2], both showing a linear trend of increasing strength with decreasing temperature. Regarding the first trend, the linear behavior was continuous throughout the temperature range tested and was similar to results obtained by Soltis et. al. [3]. For the second trend, bi-linear strength behavior is observed with a flat relationship starting at the coldest temperatures tested and ending between -7 and -10 °C, and a decreasing linear trend continuing to warmer temperatures, similar to the data generated by Scavuzzo and Chu [4].

The differences observed in the data in the literature raise the question of accuracy and precision. How can a designer choose a correct value for adhesion out of the literature for their particular application? Since the prediction of shedding relies on accurate data, it is currently difficult to make confident predictions in ice accretion codes; hence, deicing systems must be tested experimentally. This problem also complicates the comparison of competing icephobic materials since the possibility exists to select an inaccurate test approach that shows the most favorable results. In response, a new experimental method has been developed to investigate the problems associated with the historic ice adhesion test methods and data. This method was used to measure the adhesive strength of a large number of samples fabricated under near, true conditions within an icing wind tunnel. The efficiency of the overall set-up allows for the collection of a large number of ice specimens while also allowing for quick turn-around of the adhesion strength tests.

III. Methodology

The following is a summary of the methodology used to collect and test ice. Approximately 200 stainless steel (17-4 PH H900) coupons were fabricated and used to collect ice on an experimental (XT) model. Cleaned coupons were placed on the XT model within the Icing Research Tunnel (IRT) at NASA Glenn Research Center (GRC) and ice was deposited at conditions relevant to in-flight icing. The coupons and samples were removed from the model and placed into air-tight sample bags and placed into long-term storage in a walk-in freezer. The apparent adhesion strengths for each of the specimens were attained using the newly developed shear test fixture. More detailed documentation on the procedure used for this data may be found below, or in the Doctoral Dissertation in which this work was originally published [5]. The terminology used throughout the paper is as follows: a set of two days' time in the IRT is referred to as a campaign, while a specific icing event in a campaign is referred to as a run, and a test refers to the delamination of a sample on the shear rig.

A. The XT Model

A new set of models and specimen-holders, collectively referred to as the XT model, were designed and built for creating the ice adhesion specimens in the IRT 6'x9' test section. Each side of the XT model could hold 24 adhesion specimens (a maximum of 48 mounts can be used simultaneously in the test section). The model was used in the 24 mount configuration for this work. The coupons were mounted such that they stood 2" ahead of the main trusses of the model and were spaced 6" between centers to reduce aerodynamic interaction. Note that the XT model structure displayed some aeroelastic responses during speed-up in the form of induced Von-Karman shedding. This was evident in the form of a high level audible vibration, which occurred most prominently at approximately 110-120 knots and mainly on the clean model. The assembled model before and after icing is shown in Figure 1.

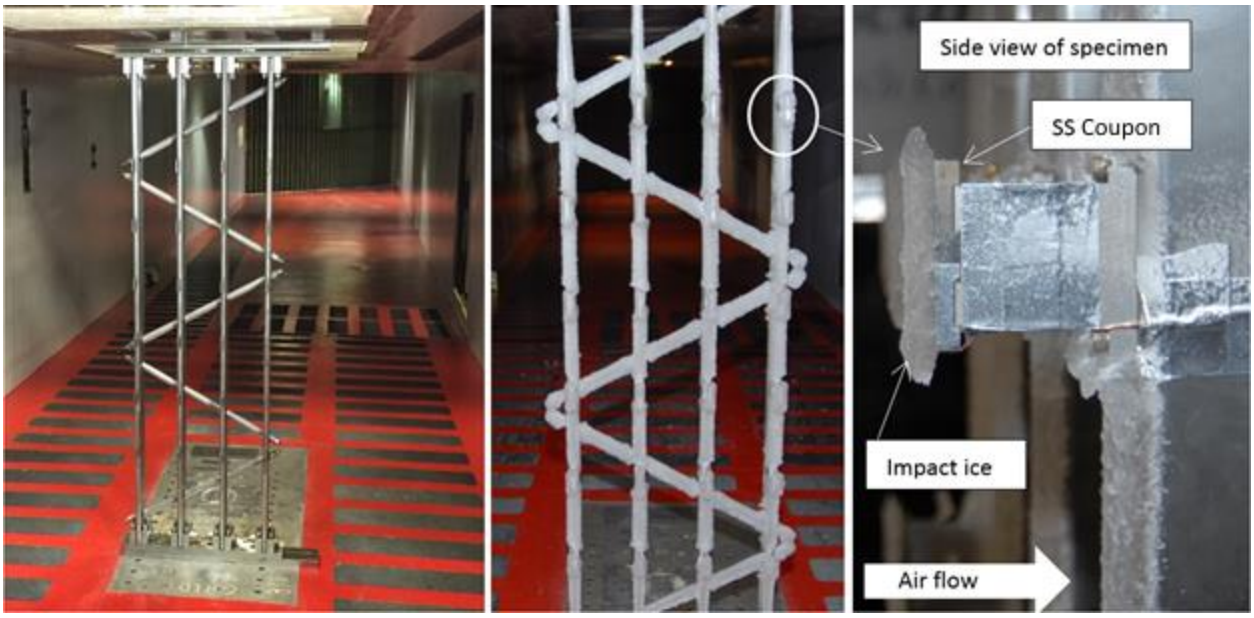

Figure 1. A single XT model in the 6'x9' IRT test section before test, without ice (left) and after test with ice (center). Mounted sample with embedded thermocouple (right).

The XT model was first used in the October 2017 Icephobics test campaign in the IRT in the 24 mount configuration, as shown in Figure 1. The samples were numbered from 1 to 24 going from left to right, top to bottom (top row was 1, 2, 3, 4, next row was 5, 6, 7, 8, and etc.). Three of the 24 mounts were reserved for dummy coupons with embedded thermocouples; these were sample numbers 4, 7, and 14 in the first campaign, and 4, 21, and 24 in the second campaign (November 2017). The dimensions of the smoothly ground, stainless-steel (SS) coupons were 2"x0.25"x0.25". Dovetail slots were cut in the back of each coupon to allow for sliding the samples into the holders on the XT model as well as for mounting within the modified lap joint shear tester (a set screw is tightened after placement to prevent movement). The front face of each SS coupon was placed perpendicular to the airflow in the tunnel to allow for ice build-up.

B. Tunnel Procedure

Four nights of testing in the IRT were utilized to obtain the samples; two days of testing in an October 2017 campaign, and two days in a November 2017 campaign. The plan for these tests was to run a velocity sweep the first night and a mean volumetric diameter (MVD) sweep the second night while also running both tests at different total temperatures. This was altered for the November campaign since samples encountered issues at the lower temperatures during the November campaign (see below). The final target test matrix for each IRT test is shown in Table 1.

Table 1. Target run conditions in the IRT by run letter.

Runs A-D completed night 1, runs E-J completed night 2.

Run	V (m/s)	Ma	T_s (C)	T_t (C)	LWC (g/m^3)	MVD
A	64.3	0.20	-9.2	-7.1	1.50	20
B	77.2	0.24	-10.1	-7.1	1.33	20
C	90.0	0.28	-11.1	-7.1	1.21	20
D	102.9	0.31	-12.3	-7.1	1.12	20
E	77.2	0.24	-10.1	-7.1	1.4	15
F	77.2	0.24	-10.1	-7.1	1.4	30
G	77.2	0.24	-10.1	-7.1	1.4	50
H	77.2	0.24	-10.1	-7.1	1	180
I	77.2	0.24	-10.1	-7.1	1.4	25
J	77.2	0.24	-10.1	-7.1	1.4	40
K	70.7	0.22	-17.5	-15.0	1.41	20
L	77.2	0.24	-17.9	-15.0	1.33	20
M	77.2	0.24	-13.9	-11.0	1.33	20
N	102.9	0.32	-17.2	-12.0	1.12	20
O	77.2	0.24	-10.0	-7.1	1.33	20
P	83.6	0.26	-18.4	-15.0	1.26	20
R	77.2	0.24	-12.9	-10.0	1.4	15
S	77.2	0.24	-12.9	-10.0	1.4	30
T	77.2	0.24	-12.9	-10.0	1.4	50
U	77.2	0.24	-12.9	-10.0	1.4	30
V	77.2	0.24	-12.9	-10.0	1.4	25
W	77.2	0.24	-12.9	-10.0	1.4	30
X	90.0	0.28	-14.0	-10.0	1.21	20

For the first campaign, ten different conditions were run in the IRT at a fixed temperature of -7.1 °C (all glaze ice). The conditions were created by varying the velocity between approximately 125 knots and 250 knots and changing the mean volumetric diameter (MVD) of the cloud between approximately 15 µm and 180 µm. The ten runs in the IRT were given letter designations from A to J.

For the second campaign, thirteen runs were completed. The total temperature was varied from -15 to -7.1 °C in an attempt to troubleshoot the issue with ice falling off of the coupons prematurely. The last two runs (W and X) were run with the cloud pulsed, either on for 10 seconds and off for 20 seconds on repeat (run W), or on for 3 seconds and off for 11 seconds on repeat (run X). This was done in an attempt to change the thermodynamics of accretion to see if the induced change in residual stresses would be significant enough to alter the problem.

Samples were cleaned with SF-77 degreaser (diluted with tap water at a 10:1 ratio) and mounted in the tunnel. After samples were mounted, they were cleaned with Isopropyl Alcohol immediately before the IRT run was initiated. After ice build-up and when removing the specimens from the IRT, the tunnel fan was kept on idle in order to keep the test section temperature relatively constant. This provided a steady breeze between 10 and 15 knots, and improved temperature uniformity as compared to a fan-off condition. While still in the tunnel, the samples were individually bagged in air tight sample bags and placed in portable freezers for short term storage. Samples were moved into a walk-in freezer for long-term storage at a temperature of -10 °C. The walk-in freezer was located adjacent to the environmentally controlled mechanical test system described below.

C. Shear Test Method

An electromechanical load frame was used for the ice adhesion shear tests. The test section of the load frame was boxed in an environmental chamber in order to control the temperature and regulate the humidity. A custom lap joint shear rig was designed and employed as a fixture to hold the samples. It is shown pictured within the environmental chamber in Figure 2.

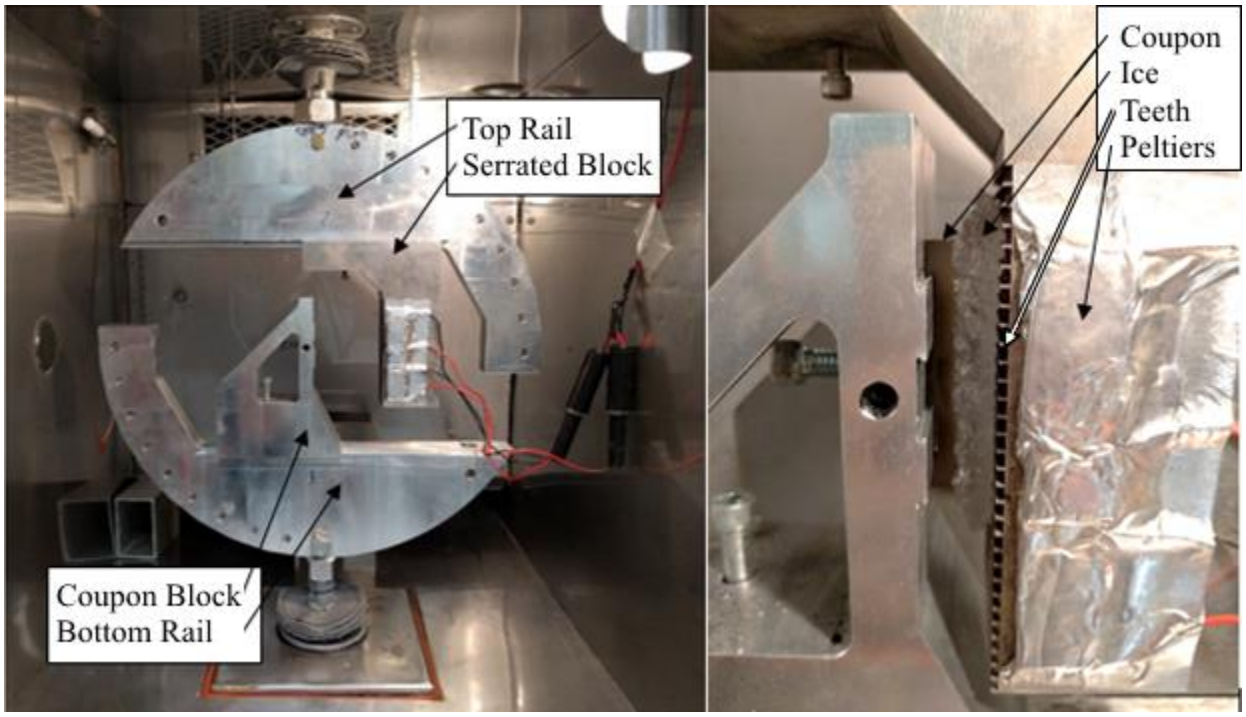

Figure 2. Custom ice lap joint shear rig (left), with ice mounted ready for test (right).

The fixture was designed such that it could be rotated to vary the state of stress at the interface, hold samples of a variety of sizes, and also place samples under compression. In this study, it was used in the 0° position in order to test a nominal mode-II failure. Ice samples were taken from long term storage in the walk-in freezer, and quickly placed in the environmental chamber while still in the air tight sample bags. The samples were then taken one at a time and placed on the dovetail rails, where a set screw was tightened to hold the sample in place. Next, the specimen was penetrated by the serrated block with metal teeth, shown at the right-most side of Figure 2. Embedded Peltier devices were used to slightly heat the teeth to allow for ice penetration. Two Peltiers were held at 24 V in series and pulled between 5.1 and 4.7 Amps (as the Peltiers heated, they pulled less current) for approximately 10 seconds (in some cases more time was used). Manual force was applied to the serrated block to push it into the ice while the heat was being applied. Removing the force when the heat was cut off allowed the fixture to relax before the ice near the teeth refroze. The heat settings were based on the minimal energy required to penetrate the far side of the specimen. Once the sample was refrozen, it was allowed to equilibrate in the chamber for at least 3 minutes before mechanical testing.

Testing was performed by pulling the serrated block upwards at a constant rate in stroke control and recording the force. The block was moved up at speeds of 0.02, 0.2, and 2 mm/min, with the baseline rate being 0.2 mm/min. At least four samples from each test were run at the baseline rate as soon as possible after the corresponding IRT run in the following manner. Run J was the last run from the first campaign and was the first tested in the lab. Batches of samples in the second campaign were tested immediately following the corresponding run in the IRT. Samples were taken from two runs at a time (five from I and J, 4 from A and B, etc.). After at least four samples were run from each IRT test at the baseline strain rate, additional tests were then run at the other strain rates. Each set of subsequent tests also included baseline rate tests to capture time-dependent storage effects on the adhesion strength.

IV. First IRT Campaign Results and Discussion

The first dedicated IRT campaign was completed on 10/2/17 and 10/3/17. A total of 193 samples were collected for testing from the first campaign in the IRT. Of these samples, 167 were used to produce results with an adhesive

failure and no obvious errors in the testing process. Repeat samples were averaged together; grouping was based on MVD, velocity, crosshead speed, and annealing time (time between cloud-off and shear test). Three different crosshead speeds were used to test samples; typical force-position recordings are shown in Figure 3.

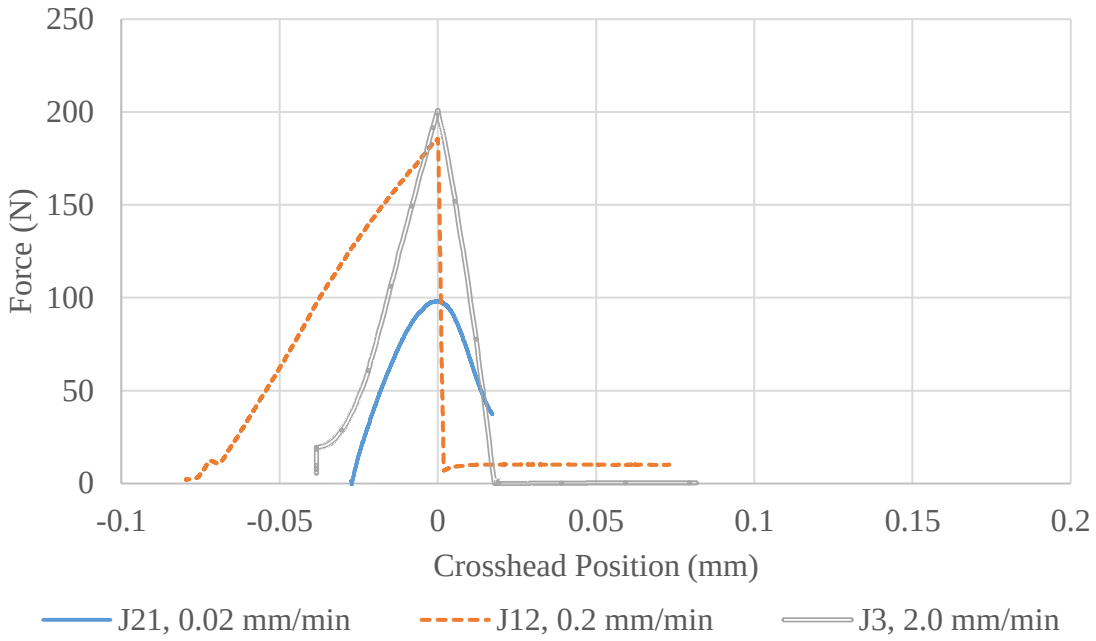

Figure 3. Typical force-position curves for three load rates.

The vertical lines at the start of loading were due to system drift before the test began. The force-position behavior exhibited in Figure 3 was typical, though in some cases rounded plots were obtained at higher speeds. In some cases, a steady force was left after the break, likely due to the sample being lightly compressed and frictional sliding occurring at the interface between the SS and ice. The next to slowest speed sample (J12) had a nearly linear response with some softening near the peak, possibly indicating some plastic deformation. The 2.0 mm/min sample (J3) behaved a little differently, with stiffening at the beginning of load-up. This was possibly due to slipping in the shear rig giving a non-linear response. The drop-off in this instance was comparatively slow, possibly due to a steady delamination of the sample, frictional sliding, or inertia in the fixture. The data for the lowest speed (J21) shows a non-linear response where the sample did not finish delaminating during the test. This test ran for approximately five minutes, and the rounded plot likely indicates a plastic response and potentially creep flow in the ice. Generally, the middle speed was considered to behave in the least-complicated fashion.

In the first set of results, the crosshead speed was varied to induce different strain rates. However, these rates were not the same as the strain rates since it will be shown that the relative motion of the coupon and teeth are not the same as the motion of the crosshead due to flexure in the shear rig and connecting rods. Since the flexure of the connecting rods varied with the force exerted on them (following Hooke's Law) the actual strain rate would have varied as samples possessed various stiffness such that stiffer samples were likely subjected to a lower strain rate than more compliant samples. This was not accounted for in the first data set since samples did not have the deflectometers mounted. No significant trend was observed with crosshead speed, and multiple speeds were omitted from the second IRT campaign analysis.

It was desired to compare the strengths based on coupon position in the IRT, however there was not enough data for a reliable comparison since most tests produced less than 20 samples. Of the three tests producing 20 or 21 samples (F, G, I), the samples were spread across two different displacement rates randomly, eliminating the possibility of direct comparison. Several samples were damaged due to handling, and many runs were completed with less than a complete number of samples since an insufficient number of SS coupons were available for filling the XT model. The average thickness for samples run from the first test was 5.85 mm, after the refreezing process.

A. Scatter

The percent standard deviation relative to the mean remained relatively consistent for the first batch of tests (< 30 hours) at 17.8%. The tests that had a downward or flat trend with annealing time tended to have much higher scatter – especially on the tests with higher annealing time; this was most prominent in A, H, and I. J also had higher scatter (and a much lower sample count), while C also showed a significant increase in scatter for the latest batch of tests even with an upward trend. The last point for J, and the first point for the A series both only had two repeats, while the remainder of the points all had three or more. The average percent standard deviation over the entire set of results from the first IRT campaign was 22.6%.

B. Velocity

The first day of testing was devoted to acquiring samples over a range of velocities while holding everything else constant. Constant nozzle settings were used for the first day such that the cloud formed from the IRT should have been identical except for velocity-related effects. The averaged data from this is shown in Figure 4.

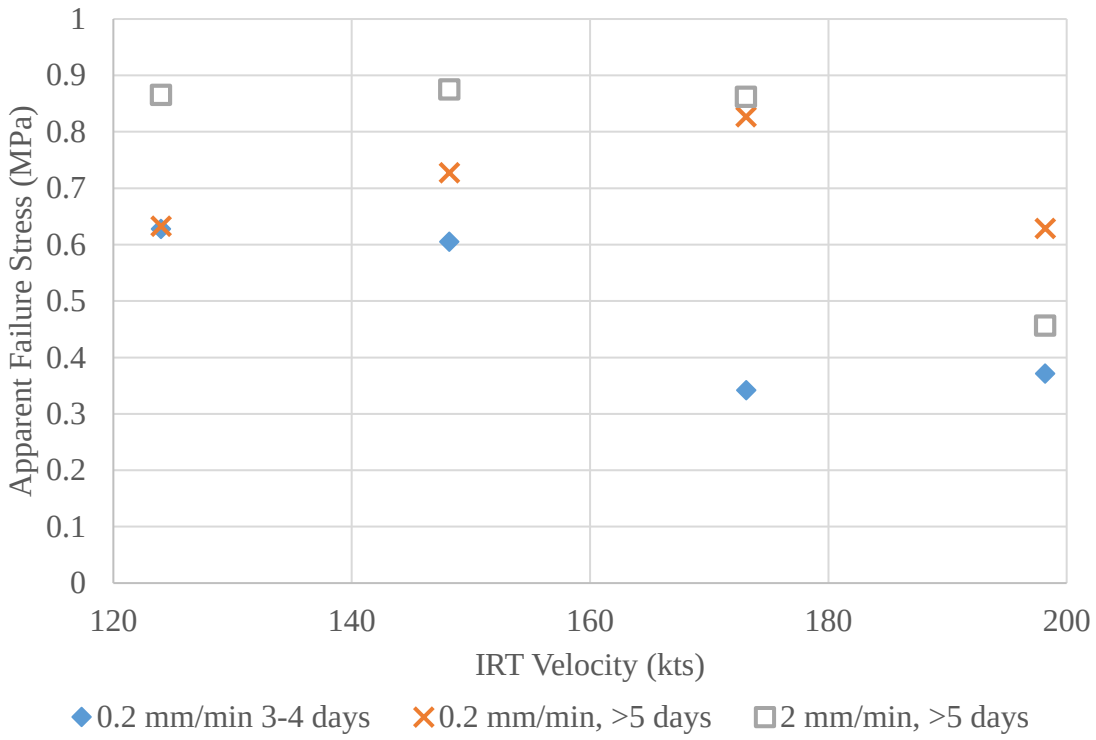

Figure 4. Average Ultimate Strength vs. Wind Speed at 25 µm MVD.

While the values were constant at lower velocities, the adhesion strength decreased at the highest velocity for each group. The data, grouped by age and crosshead speed, show different trends. The 2 mm/min data was virtually flat at the lowest three speeds, while the older 0.2 mm/min data showed an increasing trend. The data at 125 knots was from test A, which also may have produced higher-than-actual strengths due to runback, implying the existence of a peak in all curves. Differences were most prominent over the difference in time, as opposed to the crosshead speed – suggesting that annealing provided a significant effect. Stronger or different trends may have been observed for samples tested more quickly after the IRT campaign.

C. MVD

The second day of testing was devoted to changing the MVD of the cloud while holding the velocity constant at 150 knots to determine if the MVD had any effect on the data for the limited set of conditions run. The averaged data is shown in Figure 5.

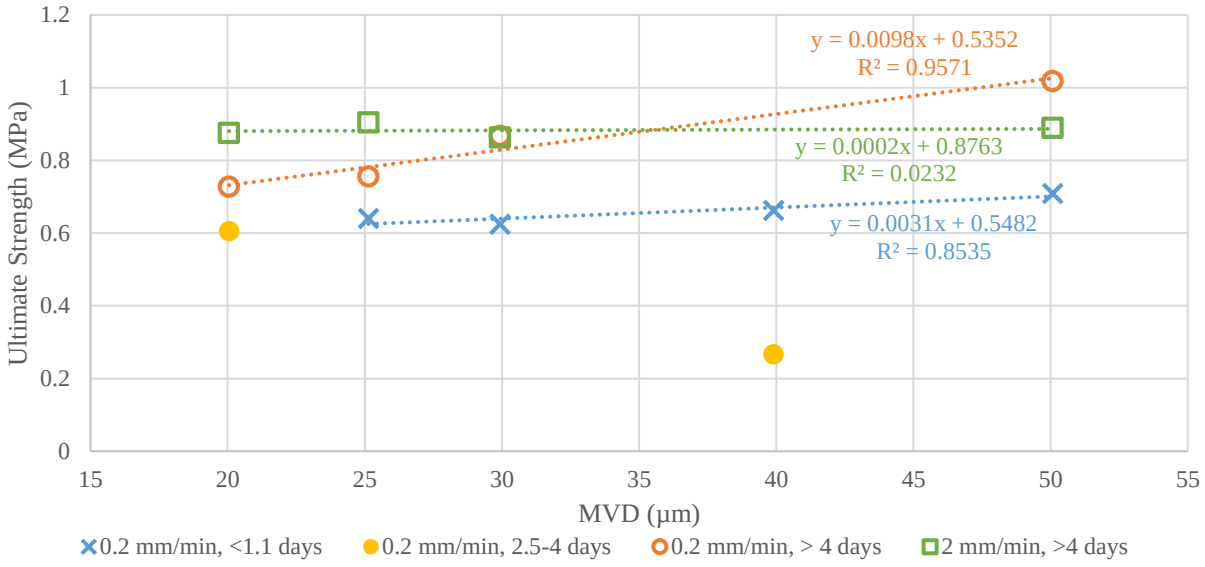

Figure 5. Average Ultimate Strength vs. Mean Volumetric Diameter of droplet size distribution, 150 knots tunnel speed.

Little effect was visible from the change in MVD in the data. In lower MVD data, a slight downward trend existed due to a spike in the lowest MVD across several tests, but no obvious trend was apparent from analysis of the data. The 15 µm data was from run E which had excessive runback on the samples, and the 180 µm data was from run H, which was an SLD case. In run H, the ice in the samples varied based on vertical position, since the largest droplets tended to miss the last two rows. Because of this the results from E and H were omitted in Figure 5.

D. Annealing

Regarding annealing time (i.e., time from IRT specimen fabrication to mechanical shear test), the earliest sample from the first campaign was mechanically shear tested 15.4 hours after cloud-off, while the last sample was tested 1094.7 hours after cloud-off. The 0.2 mm/min crosshead speed data was grouped for all series and averaged by the annealing time. This set of results is shown in Figure 6. The averaged data shows positive correlation between annealing time and strength. The scatter in the apparent failure stress was high since multiple test conditions were grouped irrespective of run conditions.

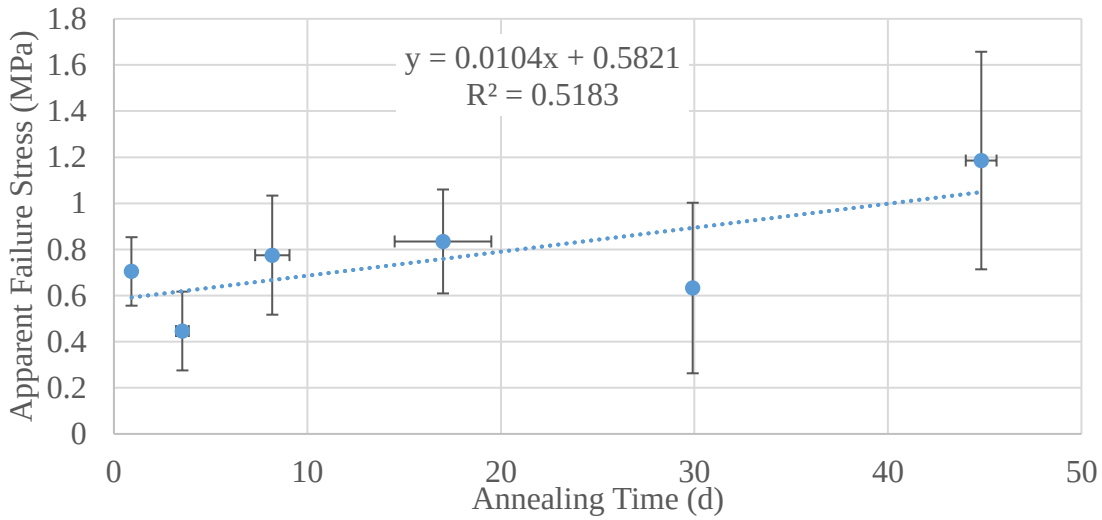

Figure 6. Averaged 0.2 mm/min data grouped by time.

The combined data showed that the apparent adhesion strength nearly doubled after annealing. Runs H and J were tested across more crosshead speeds than other runs, and so a smaller number of samples were used for these runs, possibly contributing to the downward trend of strength with annealing time for these two runs. All other runs showed a flat or upward trend of increasing adhesion strength with time to shear test. Initially, this behavior was assumed to occur due to annealing only. In older samples, it was observed that the samples had evidence of sublimation and deposition inside their storage bags, indicating that there were likely thermal variations during storage. No samples were observed to have broken off and re-adhered in this batch of results. Regardless, the samples allowed to sit for over 1,000 hours were observed to double in strength compared to those tested earlier.

V. Second IRT Campaign Data and Results

The second dedicated IRT campaign was completed on 11/20/17 and 11/21/17. One researcher was assigned to run shear tests as samples were collected to minimize the time from the tunnel being turned off to the start of the shear test for a given run. A second researcher was assigned to shave ice and record grain images and assist the Principle Investigator in transporting samples to the lab for testing. Samples were stored in cardboard boxes, grouped inside plastic bags[7]. Individual samples were stored in air-tight Whirl-Pak® bags, as in the first campaign. The objective for the second test was to repeat the first test at a lower temperature, although on the first night of testing it became immediately apparent that there was an unconsidered effect in the adhesion process when samples began to fall off on removal from the XT model.

A. Load Control Mode

Loading of the samples in the shear rig was primarily done through the control mode of the tensile tester. The position (stroke) control mode was usually used. Load drift was observed in the data in the first data set but was low compared to the values observed in the second data set. The time history of the force plot for three selected samples is shown in Figure 7.

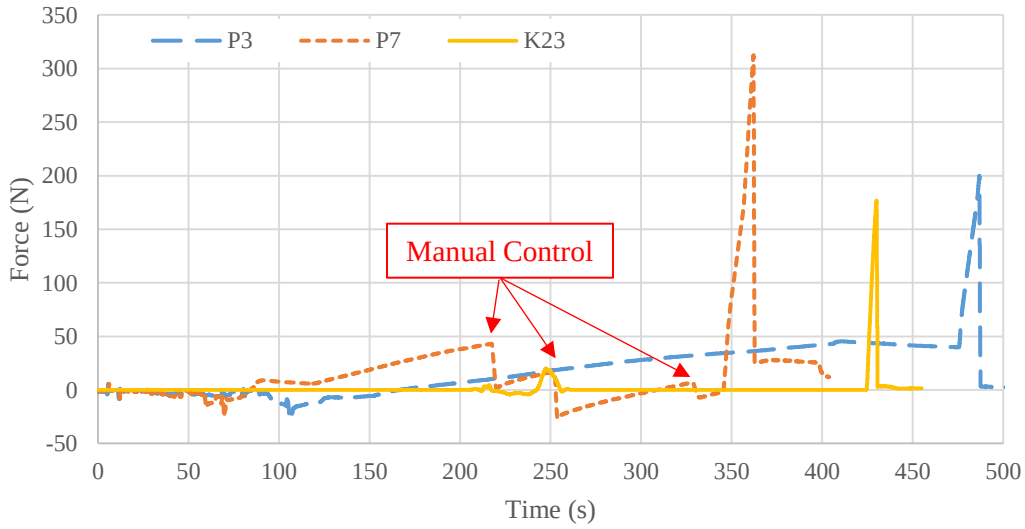

Figure 7. Force-time plot for selected samples during shear test, raw data.

Several important observations from the force-time plots are that drift was observed in the test prior to loading, likely due to thermal contraction, and some samples possessed frictional-like loading post-break. The P-series samples shown did not use force control. P3 was tested first, where the pre-load was approximately 25% of the total load. In P7, the crosshead was manually controlled to reduce the load – this shows up as sharp, nearly linear decreases in the

[7] Samples from the last run, X, were left in the portable freezer within the storage freezer used to transport samples, which provided better insulation. Markedly less ice crystals were observed in this series after storage than in the other sample sets.

force as the crosshead was moved. With K23, force control was used. The regions with erratic force (before ~120s in P3, ~90s in P7, and ~260s in K23) show the recorded forces during sample loading, melting, and refreezing while the ice was compressed. The P-series tests showed slowly increasing force after the sample refroze, while K23 did not. Different behavior in this region was observed across tests, where some cases without force control showed similar trends to K23 – a linear, near zero force while the sample was equilibrating. The lack of observed thermal expansion in some instances was possibly to be due to slipping in the coupon-coupon block connection and is discussed in the following sections. Many samples would show a constant approximately zero force after handling was finished in the mounting process. This varied with mounting procedure, where if the upper fixture was allowed to relax with the teeth still warm the force would go to zero with hands off of the fixture. In most cases, the operator pushed the serrated block into the ice, deflecting the extension rods to put force on the teeth and ice to accelerate the sinking process. If this was the case, the zero force was not observed, and the force also did not drop to near-zero post-break. This was observed in the data for sample P7 where the post-break force hovered around 25 N while the crosshead was in motion, likely due to frictional forces. The drop at the end of the P7 curve was when the crosshead was stopped right before data collection ended. Samples P3 and K23 were probably not put under lasting compression as a result of the melting and refreezing process. Allowing the fixture to relax prior to the test unloaded the compression of the sample along the horizontal axis and indicated the presence of water around the teeth since a direct mechanical connection would have resulted in a non-zero force. This also showed that the liquid water near the teeth could reduce the effect of the contraction of the fixture along the vertical axis until solidification took place, showing a potential method for reducing the effect of local contraction of the teeth on the ice. A schematic depicting the theorized geometry of these two scenarios is depicted in Figure 8.

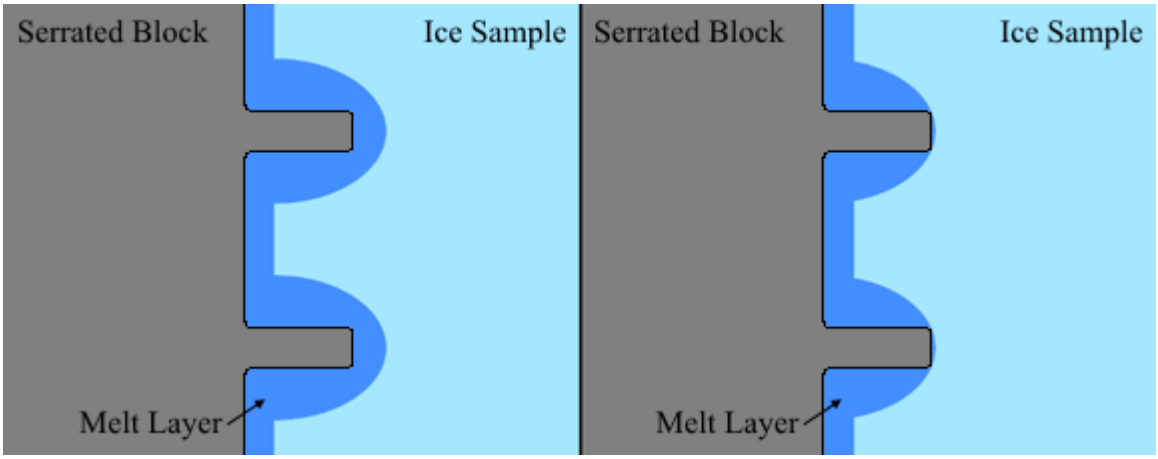

Figure 8. Depiction of idealized ice-serrated block interface. Left: interface not under compression. Right: interface under compression. Teeth to scale, water layer not to scale.

When the interface was not under compression and a liquid boundary layer was maintained, the relative motion between the serrated block and ice sample did not load the sample. If the sample was under compression, the large-scale liquid layer could not be maintained, and relative motion loaded the sample. The method that the operator used to attach the ice to the serrated block was not tracked for these tests. To minimize loading of the sample, a repeatable method should be used to produce minimal compressive forces and a repeatable liquid layer. The stress-strain curves for sample K23 is shown in Figure 9.

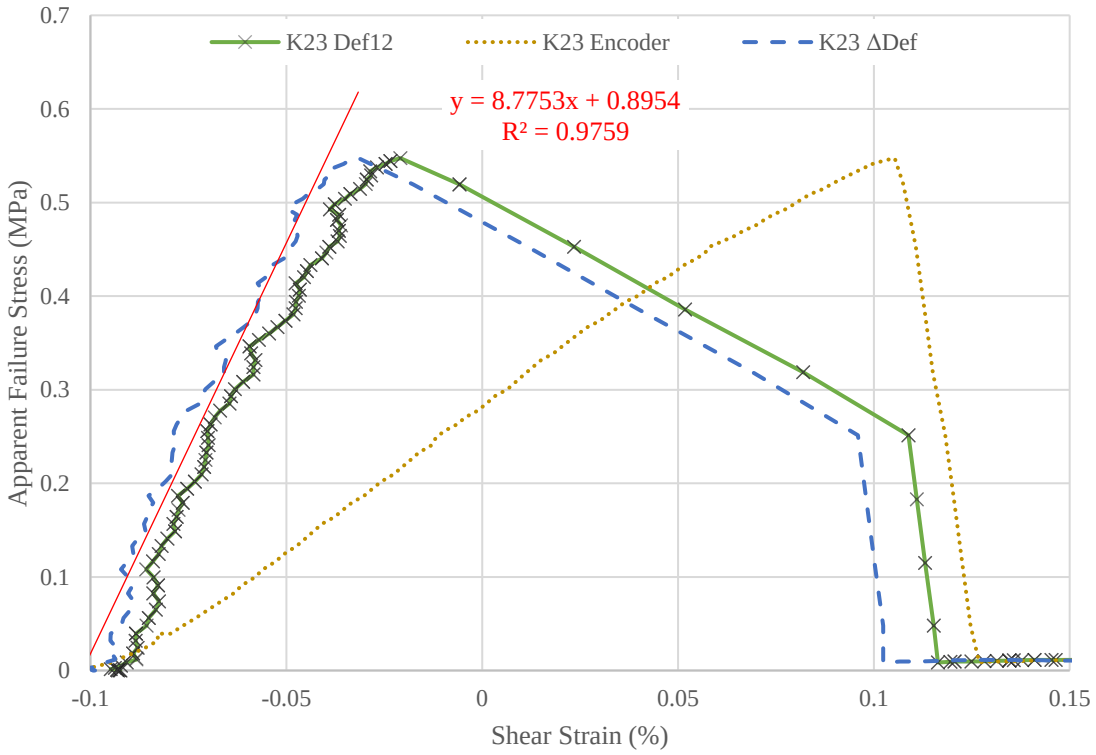

Figure 9. Stress-strain diagram using deflectometer data and encoder data.

The serrated block deflectometer (Def6, not shown) was nearly constant, which resulted in the difference between the two deflectometers (ΔDef) being a nearly uniform offset of the coupon deflectometer (Def12). The encoder data follows a much shallower slope, showing that the fixture and extension rods flex substantially during the test, offsetting the apparent shear modulus. The first linear segment showing a drop in stress on the deflectometer data corresponds to the fixture relaxing post-break and occurred over approximately 0.37 seconds. The data from the deflectometers was particularly noisy, and in some cases the deflectometers got stuck and didn't track the sample. The deflectometers still were not placed directly on the sample, and captured the deflection of the serrated block and the coupon with respect to the lower rail. The shear modulus calculation was problematic for this reason, but for sample K23 the calculated shear modulus, G, was 0.88 MPa. This was high compared to most values calculated in the control software, but only 24% of what was found in the literature – suggesting that flexure of the teeth, coupon, and serrated block collectively account for most of the deflection observed in the tests. Since better deflection data was not obtainable from the bulk of the tests, further consideration of the shear modulus was omitted from the analysis of the stress-strain diagrams obtained from the control software.

B. Scatter

No data sets from the first IRT campaign had enough data points to reasonably perform more detailed statistical analysis. To compensate for this in the second IRT campaign, two repeat runs in the tunnel were run (P was a repeat of O, and U was a repeat of S). Also, only one crosshead speed was run (0.2 mm/min). Still, only the O and P runs combined had enough samples for statistical analysis. The O and P test conditions were identical, and combined series results contained 26 samples. Other sets of data with consistent run parameters only had 13 samples or less. A histogram of this set is shown in Figure 10.

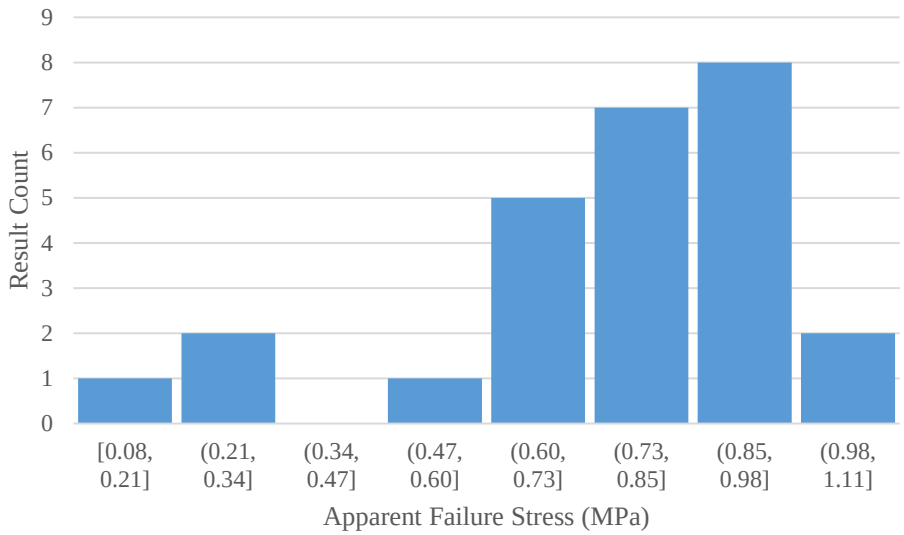

Figure 10. Histogram of results from O and P runs after being placed in storage for more than 1000 hours at 10 °C.

The lowest three values in the O and P data sets are probably erroneous since something likely occurred during the test process to damage the samples. Damaged samples would almost certainly manifest as exceptionally low values of adhesion strength, and so the strongest samples in the group should best represent actual values of adhesion strength assuming that the flaws were not inherent to the icing process. This was almost certainly not the case since samples were observed to be damaged in-situ but may serve as a reasonable approximation for most applications where damage is less likely to occur during the icing process. Samples from both O and P had moderate runback, as well as the R set of samples.

To compensate for these low values in the analysis, data from the second IRT campaign was reduced in several ways. Repeat data points were averaged, and the standard deviation was determined. The process was repeated removing low-end outliers from the data set, specifically all data one standard deviation beneath the mean ($<\lambda-\sigma$). Maximum values were also compared. Percent standard deviation values for each method of reducing the data are shown in Table 2.

Table 2. Percent standard deviations of data from IRT campaign 2.

Test	λ_{time} (h)	Count	Σ_{raw} (%)	$\Sigma_{\lambda\text{-}\sigma}$ (%)
L	2.22	3	33.8	3.1
M	0.74	1		
N	0.85	3	43.8	8.4
O	0.87	5	39.1	17.4
P	0.64	2	21.4	21.4
R	2.51	5	72.6	28.2
S	1.07	6	72.8	56.6
T	1.14	5	41.6	30.8
U	0.78	3	8.8	8.8
V	0.85	4	29.9	13.7
W	0.64	5	21.2	13.1
X	0.65	5	37.2	37.2
U	162.21	5	22.6	13
V	158.64	2	8.5	8.5
K	1366.07	9	29.4	15
L	1366.44	10	21.1	19.3
M	1364.39	6	27.6	19.7
N	925.62	3	68	17.5
O	1281.72	13	15.8	9.9
P	1200.91	15	51.3	17.6
R	1352.69	11	17.6	12.3
S	1340.81	11	33.6	23.2
T	1333.63	13	17.8	11.6
U	1316.71	2	6.6	6.6
W	1267.39	8	39.8	30.9
X	1296.23	13	29.8	15.5
Average		6.46	32.47	18.37

The values of the percent standard deviation for the raw data rose to 32.5% from 22.6% in the first campaign, an increase of 44%; this was likely due to several factors. Samples in the second test were obviously damaged in-situ with partial delamination occurring, and thicknesses in the second test were more inconsistent, but also much larger on average. Larger data sets were used in the second test which may better represent the scatter inherent to the problem.

C. Preliminary Delamination and Thickness

Trends in the literature suggest that adhesion should be stronger for ice, impact or non-impact, as the temperature decreases [1], but samples were observed to fall off at the slightest disturbance where similar runs at warmer temperatures produced robust samples. Data on the number of samples surviving (of 21) into the testing process is shown in Figure 11.

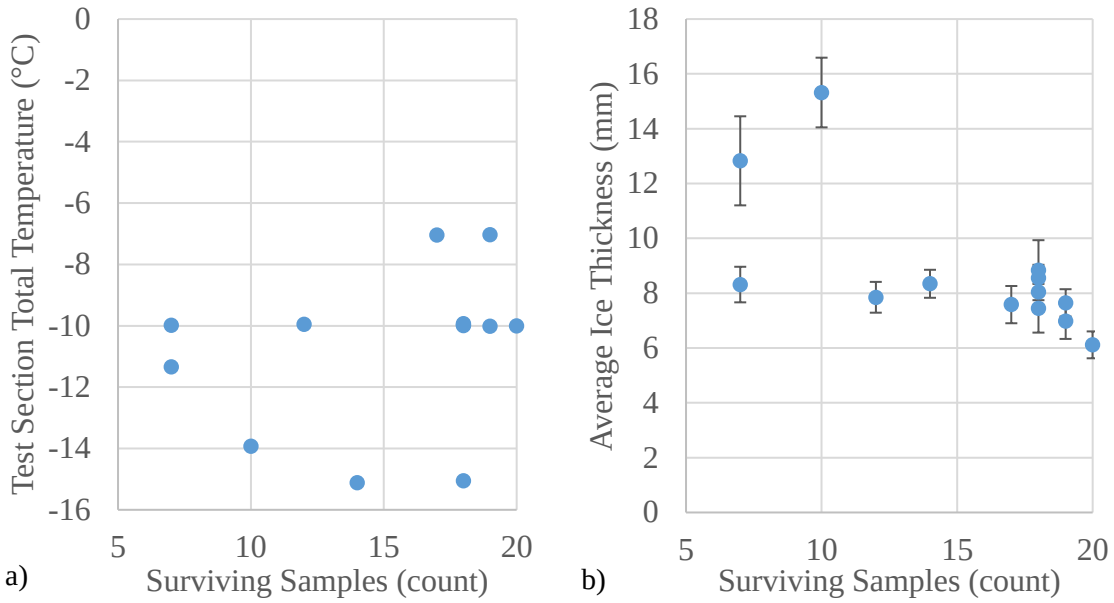

Figure 11. a) Test section temperature vs. sample count. b) Average ice sample thickness vs. sample count.

Several samples did not survive into testing due to operator errors (such as dropping samples on the test section floor[8]). The data shows some effect with temperature, where colder temperatures resulted in more broken samples. The data shows a stronger trend with thickness, where thinner samples were more likely to survive. It was hypothesized during the test that thermal stresses were expanding or contracting the ice since vibrational loading and bending of the coupons from the set screw configuration did not change significantly from the first campaign. It was unintentional that thicker samples were obtained during the second test, where average thickness for samples run from the second IRT campaign was 8.29 mm, a 42% increase from the first test. Thicker samples likely resulted in stronger residual stresses, and a stiffer specimen increasing stresses from bending of the coupons during removal. It was noted that many of the broken samples had a pattern on the interface showing lines near the edges.[9] This pattern matched a pattern of frost formed on the samples which was observed post-test, an example of which is shown in Figure 12.

Figure 12. Frost on sample K11 (top) and W6 (bottom). Some frost sublimated before pictures could be taken.

These patterns were likely due to a sublimation and frost cycle which occurred on a delaminated section of ice. Sublimation was observed to occur in sample bags in storage since small particulates of ice would form detached from

[8] The two IRT campaigns were run with the fan on idle, which made handling samples difficult due to the wind and low temperature, while thicker gloves lowered finger dexterity.

[9] Images were taken but the quality of the images were too poor to document the shape on the ice.

the sample. This effect was observed to be reduced by insulation, though not eliminated. Frost patterns were observed on the X series samples more prominently than in other tests, which was well insulated while stored. These frost patterns were also observed before storage in the freezer. This pattern was not consistent with bending of the sample, since the ice would form with the set screw in place, and when it was removed, the flexure of the coupon would pull the middle of the coupon away from the ice – tending to delaminate the ice in the middle. It was possible that frost only formed in the IRT and was removed in some cases from the sublimation-frost cycle in storage. This would make sense considering the temperatures of the samples and of the coupons. Even if the scenario described was what occurred in the tunnel, it was observed that samples could reattach to the surface after a sufficient amount of time. At least three samples showed relative motion between the ice and coupon while in storage and were taken out of storage bonded together. An example of this is shown in Figure 13.

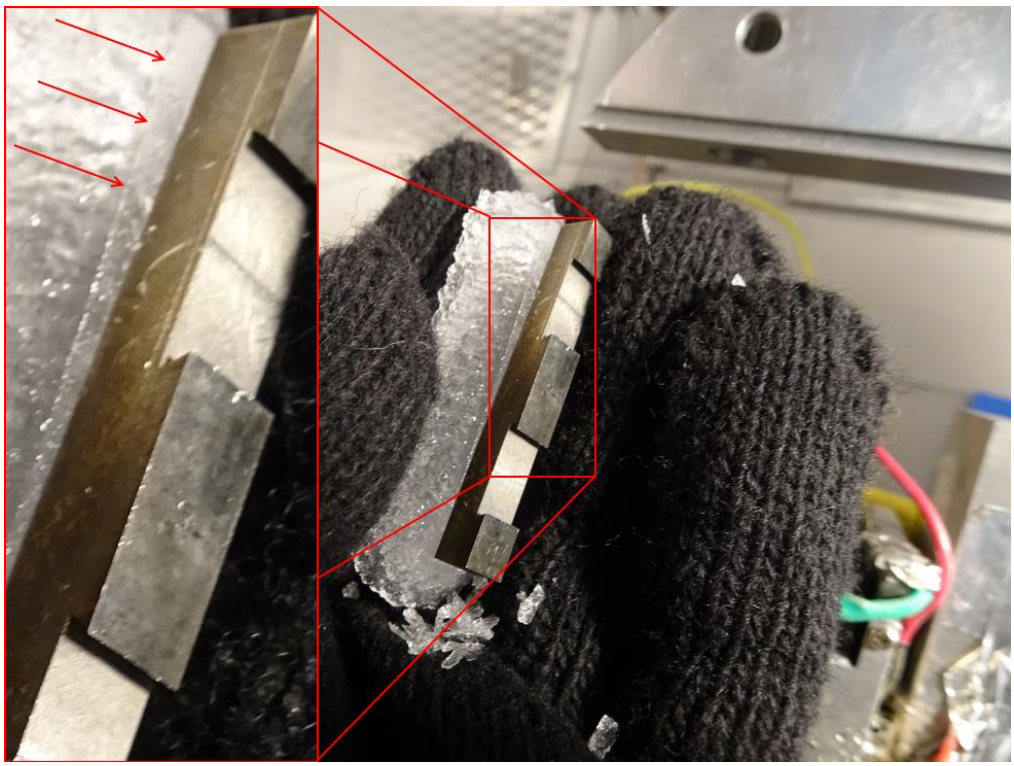

Figure 13. Sample W13 showed relative motion between the ice and coupon and was bonded on removal.

This was observed in two other samples to a similar extent and may have occurred to a lesser extent in other samples. It was unknown whether the ice stayed attached during the process, or if it slid. It was possible that the mechanism for reattachment was the same as observed in the preliminary testing. Two samples that had a large dislocation all showed significant amounts of sublimation, however this was observed to a small extent in an X series sample which had only small amounts sublimation. All samples had sat for nearly two months before this was observed. Some of this frost for the W13 sample can be seen on the glove in Figure 13 beneath the sample. While W13 was tested, samples that had large dislocations were deemed questionable and excluded from the bulk of the analysis. W13 recorded as a good break with an ultimate force of 83.1 N. S19 also had a large amount of sliding (good break, 71.1 N), as well as light sliding in X16 (good break, 198 N). The values for S19 and W13 were low for their groups, while that for X16 was near the peak value recorded for the X series. Most of the X series results had visible frost, and X16 was included in the analysis. Frost was also observed in the K, L, S, and W tests to a lesser extent. It was possible that frost occurred but was not observed on shear tests before 5 PM 1/15/18 since operators were not aware to check for it. Finally, the effect of sample thickness on the apparent adhesion strength was investigated; the data from this analysis is shown in Figure 14.

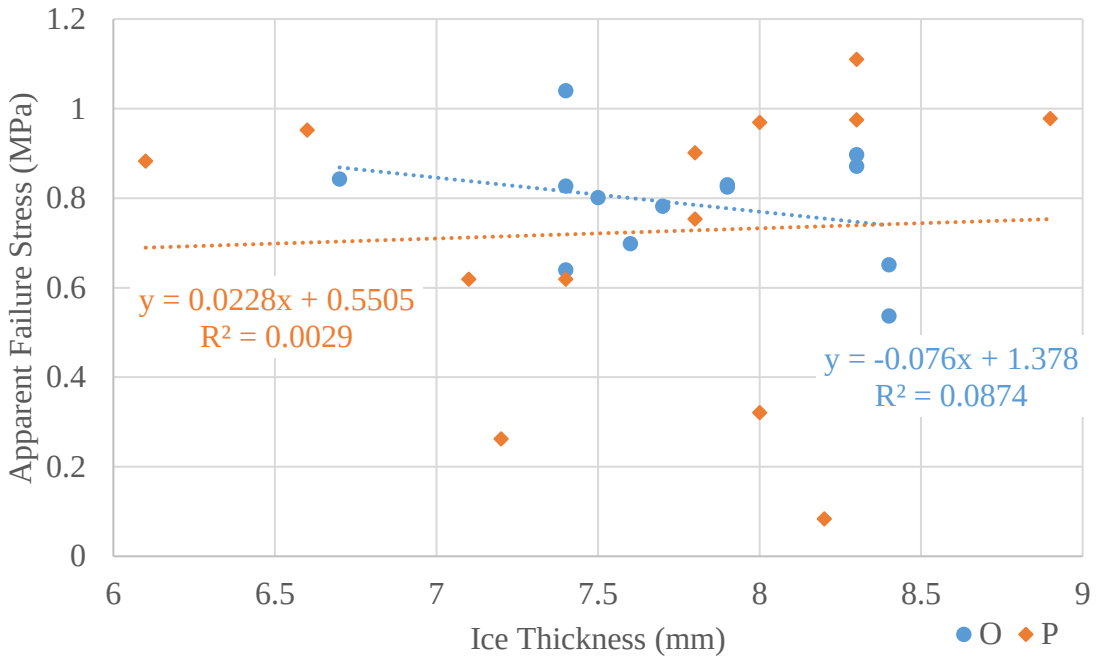

Figure 14. Failure stress vs. sample ice thickness. Runs O and P (-7 °C, 20 µm, <65 d) individual repeats.

Thicker samples should experience a lower shear rate at a fixed crosshead speed, and a fixed crosshead speed of 0.2 mm/min was used for all samples in processing the results from the second IRT campaign. The data shows little effect due to the increase in thickness, except a slight downward trend. This wasn't universal, and the trend was usually small compared to the noise in the test. From the literature, a lower strain rate should result in lower adhesion, but the effect should be observable only on the scale of orders of magnitude of strain rate variation. Further, the change in geometry resulted in different stress concentrations, an effect which was not accounted for which could show a false trend. The slight downward trend may also have been caused by variable partial delamination, where thicker samples were more likely to delaminate further resulting in a false trend in the data.

On the second night of testing, rough-cut acrylic samples were tested to help determine the cause of the preliminary delamination. Acrylic has a larger coefficient of thermal expansion than ice or steel, and a lower modulus of elasticity than either. All acrylic samples were placed in coupon slot #3. Only three were successfully tested; these were samples R3a, U3a, and V3a, which had ultimate stresses of 0.58, 0.065, and 0.105 MPa, respectively. The average failure strengths for the stainless-steel samples of the R, U, and V sets tested on the same day as the acrylic samples were 0.14, 0.27, and 0.079 MPa, respectively. R3a and V3a were tested on 11/21/17, while U3a was tested on 11/28/17. The data, while likely not statistically significant, implies that the adhesion strength was higher on the first day for the acrylic samples than for the steel samples, but lower a week into storage. Regardless, several acrylic-ice samples were broken in transit, similarly to the stainless-steel samples. This indicated that a mismatch between the samples coefficient of thermal expansion was not a likely cause of the preliminary delamination. The set screw force was also likely to be lower on the acrylic samples since they were softer and could deform more freely – operators tended to put less torque on the set screws and less torque was needed since the screws tended to dig in more than with the stainless-steel coupons. However, it was observed that some samples were stronger than others, and many fell off after the set screw was loosened. Since only one sample fell off with the tunnel running (in the cloud-off condition) out of 13 runs, each with 24 samples (three dummy samples for the thermocouples), it was regarded as unlikely that vibrational loading was significant; however, it is planned to instrument the XT structure with accelerometers in future testing to verify the loads.

D. Test Section Temperature

While the test section temperature was variable, the storage and testing temperature were fixed at -10 °C for both campaigns since the sample temperature while the cloud was on in the IRT was unknown. It was determined that the temperature of the samples varied dramatically during the spray. This was shown by the coupon temperature during the spray for run K, which is shown in Figure 15.

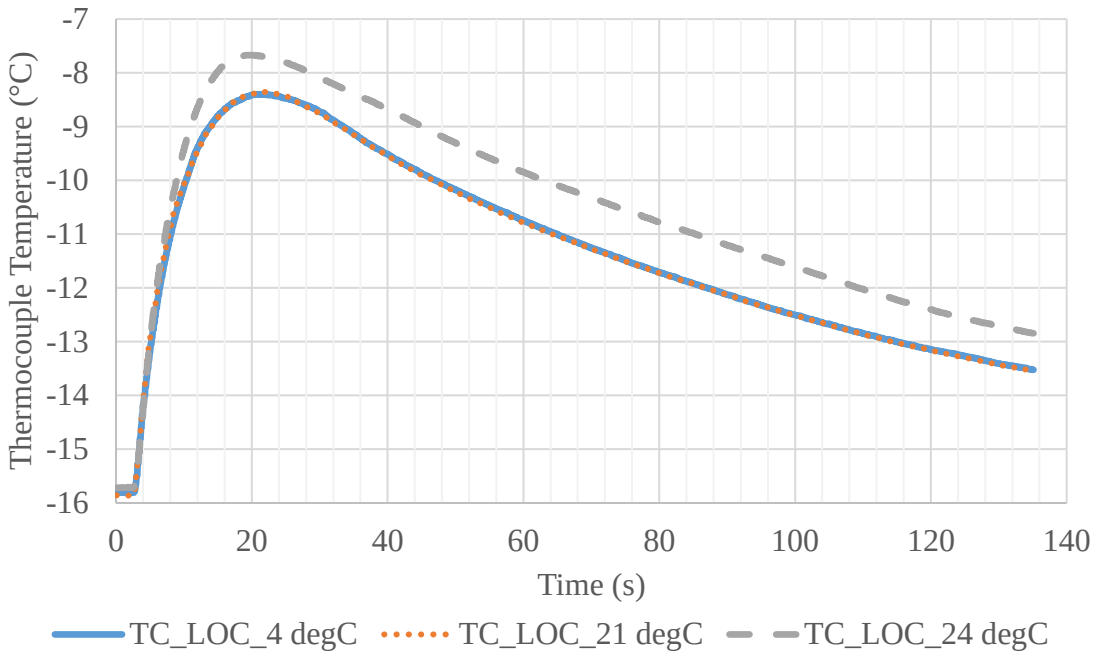

Figure 15. Temperature profile of three coupons in run K during spray.

The three thermocouples used in each IRT campaign were placed in coupon slots 4, 21, and 24.[10] In all cases, it was observed that the maximum temperature recorded occurred shortly after the onset of the spray and was always approximately halfway between the initial coupon temperature and the equilibrium temperature. This was likely a coincidence due to the placement of the thermocouple.[11] The thermocouple embedded in the coupons was not representative of the ice temperature. All conditions run for the first two IRT campaigns were glaze conditions, where the impinging droplets form a liquid film that freezes to form the ice. In glaze conditions, the latent heat release from formation is not sufficient to completely freeze the water on impact, which results in the film. The temperature of the ice on its outermost layer was thus almost certainly 0 °C, and as new ice formed over the initial layer at the interface, the interfacial temperature started to cool back to ambient conditions. If ice partially delaminated during this process, the temperature across the delaminated region would not be continuous, with the ice side warmer than the coupon. Local mass transfer could then occur between the ice and the coupon, leaving marks on the ice and frost on the coupon. A parametric plot of the averaged adhesion strength data compared to the test section total temperature is shown in Figure 16.

[10] Slots were labelled left to right, top to bottom in numerical order, such that the top row consisted of slots 1, 2, 3, 4, and the second row of 5, 6, 7, 8, and so on.

[11] Thermocouples were embedded 1/16” beneath the center of the front face of the coupons.

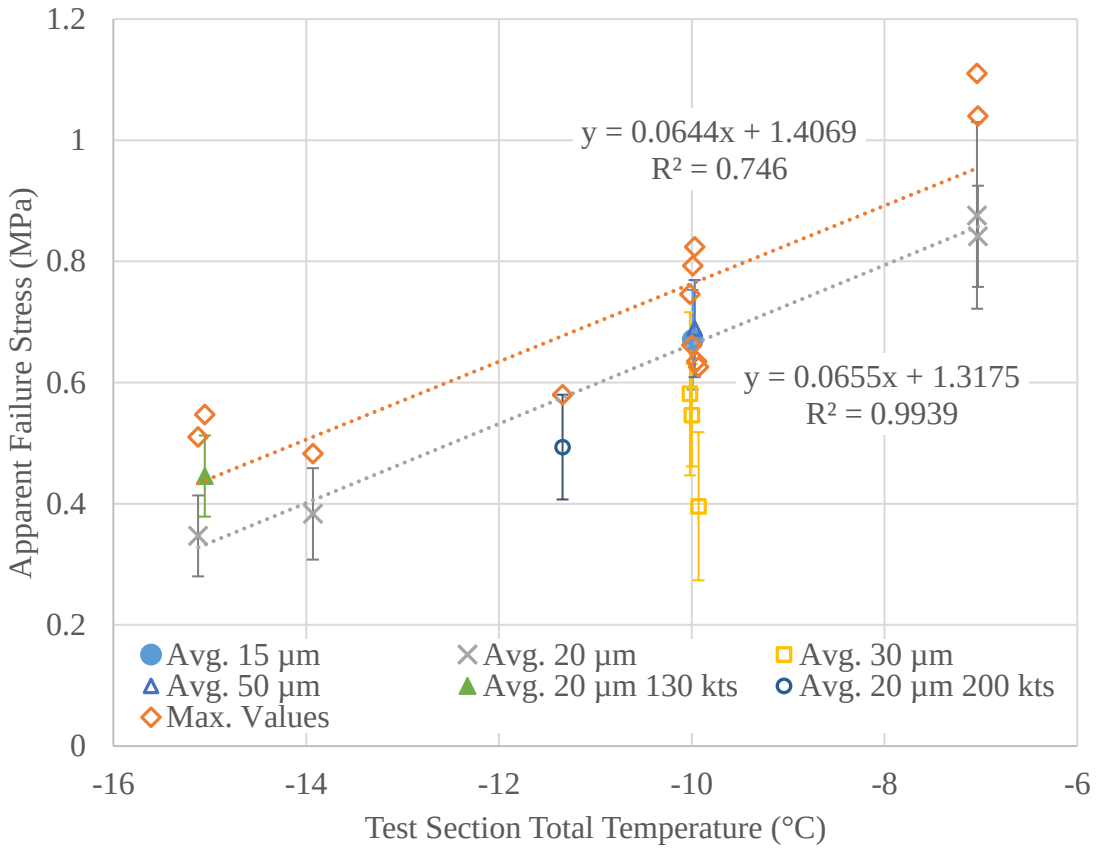

Figure 16. Parametric analysis of IRT campaign 2 data, using data > λ-σ for averaged results. Long-term storage results. 150 knots unless otherwise marked.

Data with less than 900 hours of storage time was excluded from this parametric analysis, as was data with less than four repeats (except from the maximum values data set). The original intent was to run an MVD sweep and a velocity sweep, but a temperature sweep was performed to help troubleshoot the problem of samples falling from coupons. The data showed a strong correlation with the test section temperature, possibly due to increased preliminary delamination. The highest points were from tests O and P, which exhibited moderate runback and likely artificially raised the observed adhesion strength and also probably prevented the possibility for preliminary delamination. The R run also had runback, which was the solitary 15 µm data point. Too few points were taken to obtain a strong correlation from velocity, but the singular 130 knot test point was above the 150 knot trend, and the singular 200 knot test point was below the 150 knot trend suggesting a downward trend with increasing velocity. MVD appeared to have no effect on the data since the single 15 µm and 50 µm test points fell within a standard deviation of the 20 µm trend, which was consistent with the data from the first IRT test. The data from samples stored for less than 900 hours (nominally on the same night as the corresponding IRT tests) is shown in Figure 17.

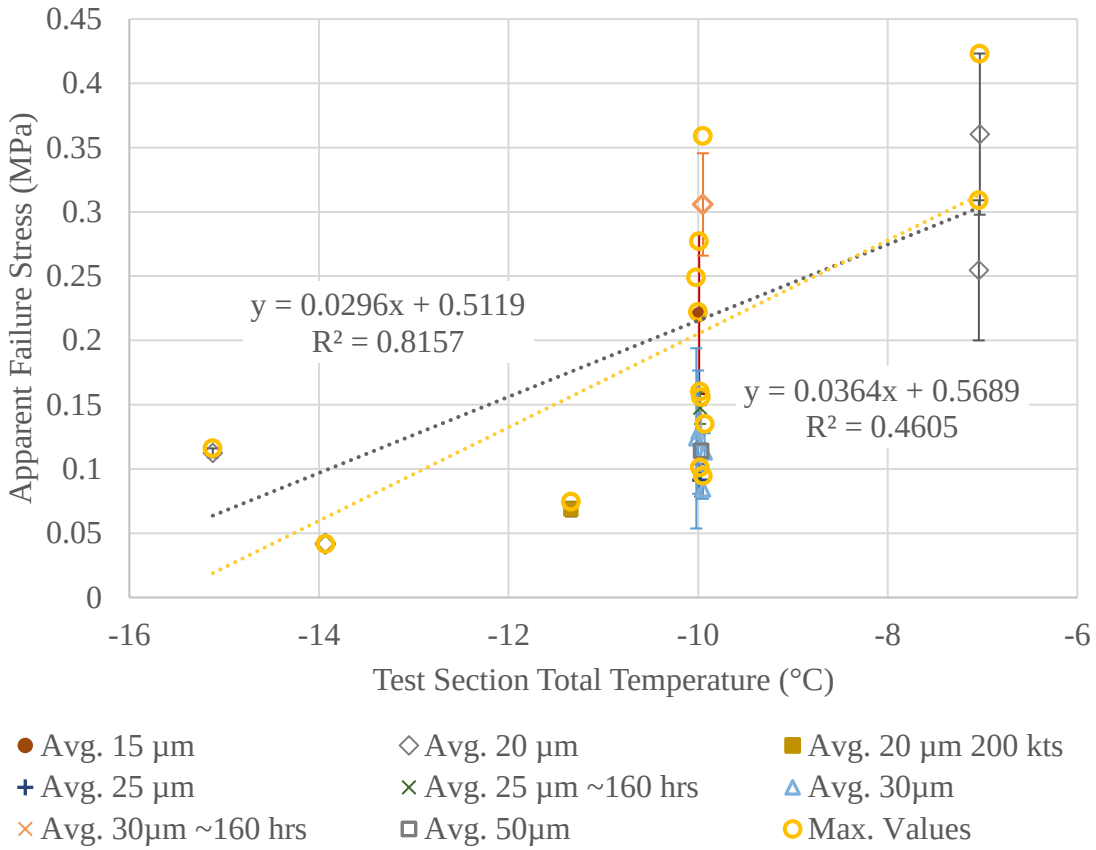

Figure 17. Parametric analysis of IRT campaign 2 data, using data > λ-σ for averaged results. Short-term storage results.

The same trends present in the long-term storage data are present in the short-term data. The one case with enough data points for a trend was the 20 µm MVD case, which showed a weaker trend with a lower slope than the long-term storage equivalent data. The maximum values showed a similar trend, also with a smaller slope than the long-term data. Both trends were poorer fits than the long-term data fits as well. The 30 µm MVD data ranged from lower to higher values of shear stress at failure from the U, W, S, and X cases, respectively. W and X were pulsed cases, with X possessing a smaller pulse time. Ice in both W and X IRT runs were notably more difficult to remove from coupons while they were still mounted in the IRT test section but fell very close to the values from the S run in initial testing. Standard deviations covered a much larger range in the early set of tests, with the warmer temperature data exhibiting higher scatter. The trend obtained in the data was the opposite of what was expected from the literature, not accounting for residual stresses in the ice. The difference was thought to be due to the difference in geometry used for the test, where the flat geometry used in this sample possibly resulted in samples delaminating partially from the edges. In the data in the literature where an opposite trend was seen for impact ice, curved airfoil surfaces were generally used [1]. The difference in geometry and the residual stresses theorized would cause pealing in these tests and clamping in those showing an opposite trend, potentially explaining the difference.

E. Attachment Temperature

Thermal imaging was performed in an attempt to measure the delay between the refreezing cycle at the interface between the ice sample and the teeth on the shear rig and the return to equilibrium (see Figure 2). One series of images is shown in Figure 18, with Time = 0 seconds corresponding to the first image being taken after the heater was shut off.

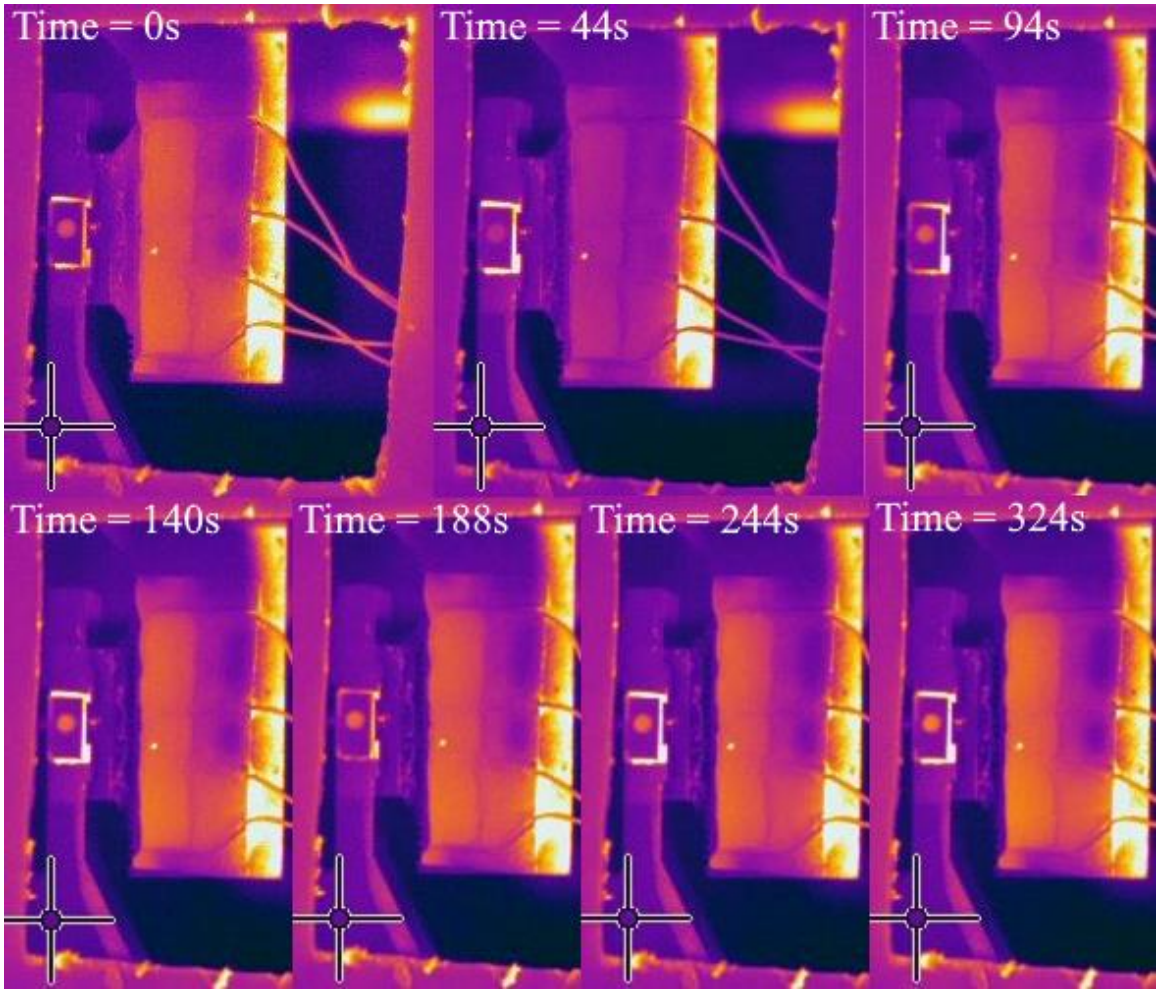

Figure 18. Thermal images of ice melting, with time shown in top left of each frame.

Several issues were observed in the imaging. Spurious temperatures were observed, possibly because the spray paint and tape were not thick enough to fully absorb radiation from the aluminum bodies they were applied to. Evidence can be seen in the tape on the coupon block, the small rectangle with the bright circle in the middle – where the circle outlines a threaded hole in the block. Separate temperature readings indicated that the block temperatures were warmer than the air temperature. While flat black paint was used, it was possible that reflections were visible on the paint or signal was transmitted through the paint. Regardless, the ice showed visible heating in the first frame (time = 0 s), and returned to near equilibrium prior to 140 s. To measure the temperature more directly, several surface mount probes were mounted to the teeth of the serrated block before continuing testing on the remaining samples from the second test. An example set of data from these probes is shown in Figure 19.

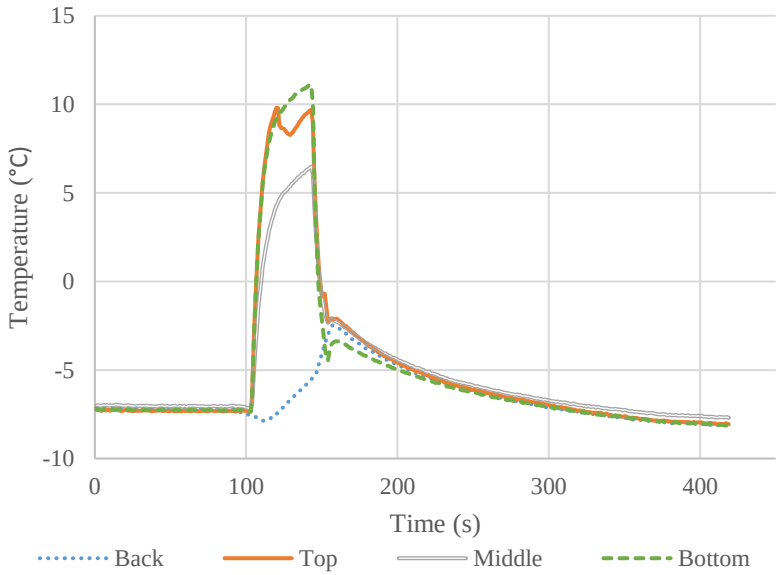

Figure 19. Temperature history for sample K23 during shear test. 40s heat, 10s cool.

The average required heating time prior to the installation of the thermocouples was 24.8s, while the average heating time after the installation rose to 65.9s, showing that they increased thermal resistance by a significant margin. Higher heating times resulted in longer required equilibrium times. The process was modified with the probes in place to start the test once a set temperature was passed. These equilibrium temperatures were between -6.8 and -7.8 °C. Warmer temperatures were used earlier in testing before it was discovered that the warmer equilibrium temperature observed was due to the cyclical opening of the glove ports in the chamber. The process was modified to keep the ports closed more frequently, and colder temperatures were used to start the test. This was recorded where applicable in the comments for the data set.

The temperature plots also show that the middle probe typically registered cooler temperatures during heating than the other probes. This was due to the presence of a strut connecting the front plate to the main block, allowing heat transfer between the teeth and the block. The bottom temperature also was lower than the top since it was connected more directly to the rail, giving lower thermal resistance between the body of the block and the teeth than at the top probe.

Several side effects likely were present from increasing the heating time of the block. The selection of aluminum for the serrated block was made due to cost, however using aluminum for the teeth was likely problematic since aluminum has a relatively high coefficient of thermal expansion, and when the teeth cool they likely compress the ice along the vertical axis. The possibility for this to not occur was if the water at the teeth did not refreeze prior to the teeth reaching equilibrium. The water freezing to hold the ice to the serrated block was observed to lag behind the temperature of the teeth since the loading reported from the load cell was nearly zero until the ice froze to lock the serrated block in place. Once locked in place, the sample would load due to thermal contraction of the fixture. Increasing the heating increased this contraction and slowed the cooling process once the teeth temperature dropped below 0 °C, as can be seen in Figure 19. Slowing this likely increased the clamping on the ice since the ice was likely locked in place for a larger temperature shift in the teeth.

Minimizing the time required to cool the serrated block back to equilibrium temperature would likely produce better results. The teeth should be thermally isolated from the body of the block to reduce heat loss and increase temperature uniformity on the teeth, and probes should be embedded to decrease the time to sink the teeth into the ice. Copper would likely be a more suitable material for the teeth due to higher thermal conductivity, a lower coefficient of thermal expansion, and higher stiffness – which would also serve to reduce flexure of the teeth.

F. Annealing

Data was grouped by the annealing time with data taken in less than four hours after the corresponding IRT run as the first group, data taken in more than 155 hours but less than 165 in the second group, and data taken in more than 1100 hours as the third group. Data was not available at intermediate times due to downtime with the shear rig test stand and scheduling conflicts. The full data set grouped and averaged by annealing time is shown in Figure 20.

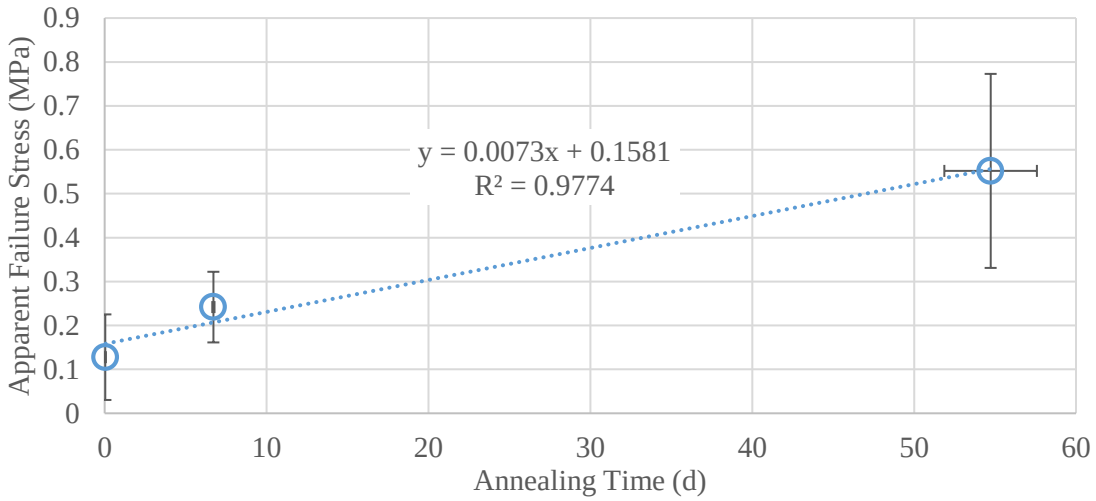

Figure 20. Apparent failure stress of all data with no outliers removed grouped by annealing time.

The trend of increasing adhesion strength with annealing time, i.e. storage time, was universal, in comparison with data from the first IRT campaign where several runs had opposite or weak trends. Both showed similar increasing trends, with the data from the first campaign having a slope of 0.0104 MPa/day, while the data from the second campaign had a lower slope of 0.0073 MPa/day. From series U (not shown), it appeared that the bulk of the change in adhesion strength happened within the first 200 hours of storage, and that the data likely reaches a plateau at longer intervals. To determine whether the samples were done aging, the individual data points used for the last groups were plotted by run with trend lines fit and no outliers removed. Only series with data points spanning multiple days of testing were used; this is shown in Figure 21.

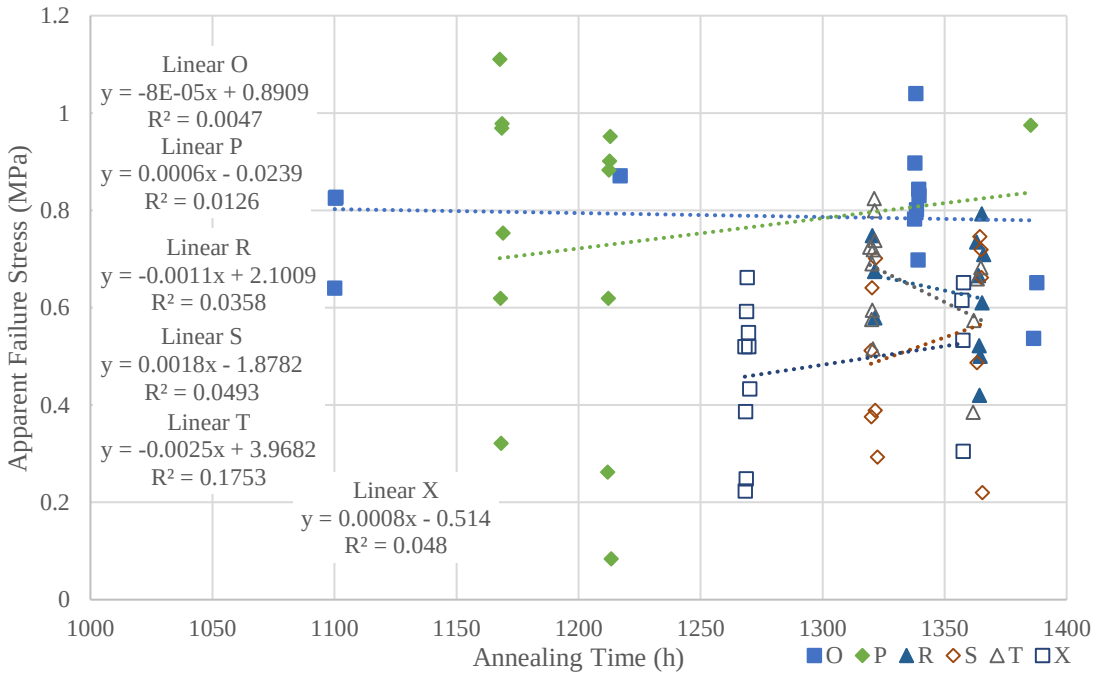

Figure 21. Longest stored data points with trend lines from IRT campaign 2.

The trend lines all have very low slope (and poor fit), but the ones with the longest span between tests had the flattest trends. This leads to the conclusion that samples were not significantly changing while aging after 1000 hours of annealing. Scatter was significant and was the likely cause of the slope in the trends observed. The observed changes samples from both test campaigns strongly suggests the presence of residual stresses in the ice. This was in good

agreement with the observation of samples delaminating in the test section, and the measured temperature changes in the ice specimens.

VI. Conclusions

A new test method was developed to measure the adhesion of ice that was a modified version of a lap-joint shear test. In addition, a new approach was developed to attach the free surface of the ice to the lap-joint fixture that was enclosed in a temperature and humidity controlled chamber. This test methodology provided several improvements over other adhesion test approaches used for impact ice, including the ability to record a stress-strain curve in a test with a more uniform stress distribution than found in pusher-type fixtures. The shear fixture also allows for running mixed-mode configurations as well as compression of the ice during mode-II testing. A new wind tunnel model for holding the SS coupons during ice accretion was designed allowing for the simultaneous fabrication of up to 48 ice adhesion samples in a single IRT run. This model was successfully used to complete two campaigns in the IRT that produced the ice adhesion coupons tested here.

A comparatively large data set measuring the apparent adhesion strength of aircraft relevant impact ice was taken for the purpose of allowing more detailed analysis into the phenomena of ice adhesion, and the methods used to measure it. The displacement rate was controlled across the data set and three crosshead speeds were used in testing the samples, each an order of magnitude apart. Flexure in the shear fixture was documented. The variations in the stress-strain curve was discussed as a function of the strain rate, showing the effects of plasticity on the data at low speeds and dynamic concerns at high speeds. Here, stainless steel coupons were used as a baseline while also allowing for the direct comparison to available data in the literature.

While data in the literature tends to show increasing adhesion strength with decreasing temperature, a strong trend was identified showing increasing adhesion strength with increasing temperature – likely due to residual stresses from the formation process. These thermal stresses in the formation process were completely neglected in the literature and were likely hidden due to various testing deficiencies. Rounded coupons used in the literature likely experienced clamping with the ice contracting on the curved surface, while flat samples experienced a stress concentration at the edges tending to reduce the apparent adhesion strength. Many of the samples fabricated in the IRT were delaminated prior to testing in the shear rig, which was likely due to the residual stresses and flexure in the test coupons during removal from the XT Model. Running tests in multiple sprays and with warmer secondary sprays eliminated the observed delamination, supporting the idea that thermal residual stresses were present and could be a significant and time-dependent factor in the adhesion of aircraft ice. The opposite trend in adhesion strength observed from those in the literature demonstrates that the simplistic methods used to measure the adhesion of ice may impart false trends to the "true value" of adhesion strength observed in nature.

VII. References

1. Work, A. and Y. Lian, *A Critical Review of the Measurement of Ice Adhesion to Solid Substrates.* Progress in Aerospace Sciences, 2018.
2. Raraty, L. and D. Tabor. *The adhesion and strength properties of ice*. in *Proceedings of the Royal Society of London A: Mathematical, Physical and Engineering Sciences*. 1958. The Royal Society.
3. Soltis, J., et al., *Evaluation of Ice-Adhesion Strength on Erosion-Resistant Materials.* AIAA Journal, 2014. **53**(7): p. 1825-1835.
4. Scavuzzo, R. and M.L. Chu, *Structural properties of impact ices accreted on aircraft structures.* 1987.
5. Work, A., *The Measurement of the Adhesion of Glaze Ice*, in *Mechanical Engineering*. 2018, University of Louisville. p. 268.